

Modelling the mechanics of a cylindrical magneto elastic elastomer

Sandeep Kumar¹, Udit Singh¹, Manu Jain¹, and Arpit Kumar Srivastava^{1*}

¹Department of Mechanical Engineering, Shiv Nadar University, Dadri, 201314 Uttar Pradesh, India

Abstract. Magneto-rheological elastomers (MREs) are a class of smart polymers whose light weight, softness, and high deformability make them attractive for soft robotics, biomedical actuators, and artificial muscles. This work deals with developing a finite element based coupled magneto-hyper-elastic numerical modelling of large deformations of Soft MREs under a magnetic field. We have modelled a cylindrical MRE tube. The results show that the actuation characteristics depend on the ratio. This helps in better understanding of the complex design parameters for MRE devices.

1 Introduction

State of the art magneto rheological elastomers are widely under investigation [1–4] due to their excellent properties such as ultra soft, light weight and high deformability.

These elastomers are created by embedding magnetic particles (such as iron or Fe_3O_4 [5]) within a flexible polymer matrix like silicone or polyurethane.

The blend is mixed, degassed, and cured, sometimes under a magnetic field to align the particles. The result is a soft, magnetically responsive material ideal for sensors, actuators, and soft robotic systems.

Understanding the mechanics of coupled magneto elastic behavior is essential to design and optimize the performance parameters of MREs based devices. Various efforts have been done in the past [6,7] to develop a numerical based framework for the coupled magneto elasticity. Recently, [8] has provided a numerical framework to model homogenized soft and hard MREs. Also, an annular membrane subjected to a magnetic field have been discussed [9].

All these works lay the foundation for understanding the intrinsic behavior of MREs. Unlike previous studies on magneto-elastic tubes which treat the geometry either analytically or through reduced-order symmetry, the present study introduces a magneto-elastic VUMAT implementation in Abaqus/Explicit formulated specifically for thin-walled MAE structures. To the best of the authors' knowledge, no previous published work has reported a thin-structure-specific VUMAT for magneto-active elastomers applied to a thin MAE tube subjected to time-dependent magnetic loading. There still needs a robust numerical framework to model the complex shape. In this work, we have proposed a novel coupled hyper-magneto-elastic FE based framework to model MREs based actuators as well as soft robotic devices.

* Corresponding author: arpit.srivastav@snu.edu.in

2 Modelling of Soft MREs

The numerical procedure presented here pertains to a thin hyper elastic soft MREs, across which a time varying scalar magnetic potential difference $\psi(t)$ is applied. The constitutive framework adopted for a nonlinear model closely follows the development outlined in [6].

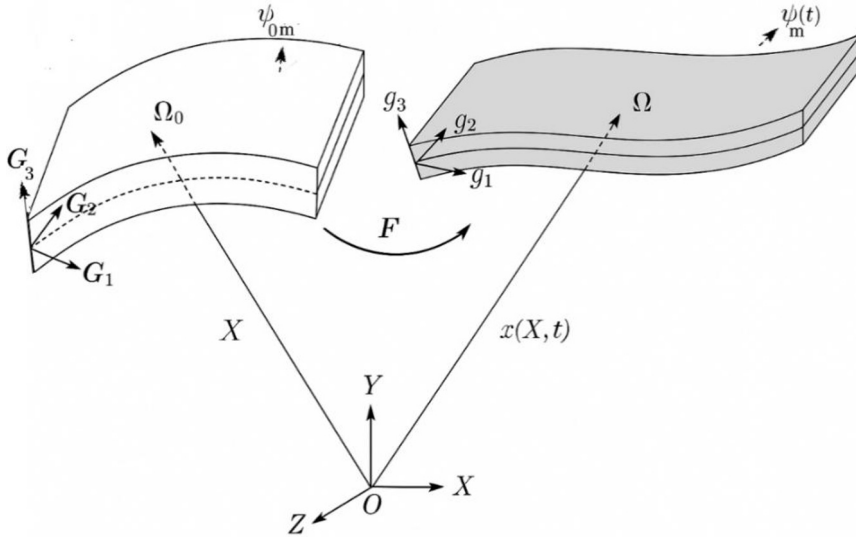


Fig. 1. Schematic showing deformed and undeformed configurations of a magneto elastomer membrane subjected to a scalar magnetic potential ψ applied across the face perpendicular to g_3 .

A point \mathbf{X} in the undeformed configuration of the thin MRE maps onto a point $\mathbf{x}(\mathbf{X}, t)$ in the deformed configuration (see, Figure 1). The deformation gradient tensor is \mathbf{F} . The deformation gradient volumetric and isochoric parts as

$$\bar{\mathbf{F}} = J^{-1/3} \mathbf{F} \quad (1)$$

Hence, the isochoric right Cauchy Green tensor becomes,

$$\bar{\mathbf{C}} = J^{-2/3} \mathbf{C} \quad (2)$$

where $\bar{\mathbf{C}} = \bar{\mathbf{F}}^T \bar{\mathbf{F}}$, $J = \det \mathbf{F}$ and \mathbf{C} is the right Cauchy Green tensor.

The current configuration of the membrane is subject to a spatial magnetic flux density $\mathbf{B}(\mathbf{x}, t) = \mu_m \mathbf{H}(\mathbf{x}, t)$ which the thin MRE membrane experiences due to spatial magnetic field density $\mathbf{H}(\mathbf{x}, t)$. Here, μ_m is the deformation independent magnetic permeability.

The components planar to membrane surface of $\mathbf{H}(\mathbf{x}, t)$ are zero. Also, we will denote $H = \psi(t)/h$, here h is the current thickness of MRE membrane.

For the development of model, compressible Ogden material is assumed [10,11] which has an additional contribution from the magnetoelastic field to the strain energy density per unit volume. Thus, the strain energy density per unit reference volume is,

$$\psi(J, \bar{\mathbf{C}}, \bar{\mathbf{B}}) = \psi_V(J) + \bar{\psi}(\bar{\mathbf{C}}) + \psi_m(J, \bar{\mathbf{C}}, \bar{\mathbf{B}}) \quad (3)$$

where, $\psi_V = K(J - 1)^2$ (4)

$$\bar{\psi}(\bar{\mathbf{C}}) = \frac{2\mu_1}{\alpha_1^2} (\bar{\lambda}_1^{\alpha_1} + \bar{\lambda}_2^{\alpha_1} + \bar{\lambda}_3^{\alpha_1} - 3) \quad (5)$$

$$\psi_m(J, \bar{\mathbf{C}}, \bar{\mathbf{B}}) = \frac{\bar{\mathbf{B}} \cdot \bar{\mathbf{C}} \cdot \bar{\mathbf{B}}}{2\mu_m J^{1/3}} \quad (6)$$

Using equation (3), the second piola kirchhoff stress is as follows

$$S_1 = \frac{J}{\lambda_1^2} \left(\frac{\partial \psi_V}{\partial J} + \frac{\partial \psi_m}{\partial J} \right) + \frac{1}{\lambda_1^2} \left[\frac{2}{3} \bar{\lambda}_1 \left(\frac{\partial \psi_m}{\partial \lambda_1} + \frac{\partial \bar{\psi}}{\partial \lambda_1} \right) - \frac{1}{3} \bar{\lambda}_2 \left(\frac{\partial \psi_m}{\partial \lambda_2} + \frac{\partial \bar{\psi}}{\partial \lambda_2} \right) - \frac{1}{3} \bar{\lambda}_3 \left(\frac{\partial \psi_m}{\partial \lambda_3} + \frac{\partial \bar{\psi}}{\partial \lambda_3} \right) \right] \quad (7)$$

$$S_2 = \frac{J}{\lambda_2^2} \left(\frac{\partial \psi_V}{\partial J} + \frac{\partial \psi_m}{\partial J} \right) + \frac{1}{\lambda_2^2} \left[-\frac{1}{3} \bar{\lambda}_1 \left(\frac{\partial \psi_m}{\partial \lambda_1} + \frac{\partial \bar{\psi}}{\partial \lambda_1} \right) + \frac{2}{3} \bar{\lambda}_2 \left(\frac{\partial \psi_m}{\partial \lambda_2} + \frac{\partial \bar{\psi}}{\partial \lambda_2} \right) - \frac{1}{3} \bar{\lambda}_3 \left(\frac{\partial \psi_m}{\partial \lambda_3} + \frac{\partial \bar{\psi}}{\partial \lambda_3} \right) \right] \quad (8)$$

$$S_3 = \frac{J}{\lambda_3^2} \left(\frac{\partial \psi_V}{\partial J} + \frac{\partial \psi_m}{\partial J} \right) + \frac{1}{\lambda_3^2} \left[-\frac{1}{3} \bar{\lambda}_1 \left(\frac{\partial \psi_m}{\partial \lambda_1} + \frac{\partial \bar{\psi}}{\partial \lambda_1} \right) - \frac{1}{3} \bar{\lambda}_2 \left(\frac{\partial \psi_m}{\partial \lambda_2} + \frac{\partial \bar{\psi}}{\partial \lambda_2} \right) + \frac{2}{3} \bar{\lambda}_3 \left(\frac{\partial \psi_m}{\partial \lambda_3} + \frac{\partial \bar{\psi}}{\partial \lambda_3} \right) \right] \quad (9)$$

The principal values of the Cauchy stress $\boldsymbol{\sigma}$, is given by

$$\boldsymbol{\sigma} = \frac{1}{J} \mathbf{F} \mathbf{S} \mathbf{F}^T \quad (10)$$

Finally, to obtain the stresses in the global coordinate system, the principal values are then transformed back to normal using a rotation Matrix \mathbf{Q} .

The above formulation is then implemented in a user-defined VUMAT subroutine in the commercial code ABAQUS.

The value of material characterization such as Ogden parameters $\mu_1 = 161$ kPa and $\alpha_1 = 1.632$. Magnetic permeability is obtained from fitting the parameters [12].

3 Results and Discussion

The above model is then used to simulate a hollow cylindrical tube actuator of thickness = h (in this case h = 1 mm). Three-dimensional four node Shell element (S4R) is used to model cylindrical tube. The length of the tube is kept as 90 mm. The outer radius R has been taken as 30 mm and 90 mm respectively. This provides two extreme different aspect ratios α is equal to 0.33 and 1 respectively. The actuator is fixed at one end while the other end is free.

These two cylindrical tubes are then subjected to a time dependent magnetic flux density $B(t)$, in the thickness direction, which is varying from 0 at time t=0 s to 434 mT at t = 1 s. The time dependent magnetic scalar potential $\psi(t)$ is calculated using

$$B(t) = \mu_m \frac{d\psi(t)}{dh} \quad (11)$$

The nondimensional parameters used to characterize the cylindrical MRE tube actuator include \bar{u}_r , \bar{u}_z , $\bar{\lambda}_\phi$, $\bar{\lambda}_z$, $\bar{\sigma}_\phi$, \bar{B} and \bar{H} . The definitions of these quantities are given in Table 1.

Table 1. Definition of the normalized parameters.

Symbol	Definition
\bar{u}_r	$\frac{u_r}{L}$
\bar{u}_z	$\frac{u_z}{L}$
$\bar{\sigma}_\phi$	$\frac{\sigma_\phi}{\mu_1}$
\bar{B}	$\frac{B}{\sqrt{\mu_1 \mu_m}}$
\bar{H}	$H \sqrt{\frac{\mu_m}{\mu_1}}$

Here, u_r = radial displacement, u_z = axial displacement, σ_ϕ = circumferential (hoop) stress, μ_1 = shear modulus of the material, μ_m = magnetic permeability, B = magnetic flux density, H = magnetic field intensity

Figure 2 (a) shows the variation of displacements in radial direction. The study suggests that this actuation is strongly dependent on aspect ratio α , for a bigger aspect ratio radial actuation will be more. The maximum value for radial actuation is around 0.06. The actual deformation shape of the cylinder is illustrated in Figure 3, where the increase in radial outward expansion is clearly visible with increasing \bar{B} , and is more pronounced for larger aspect ratio.

Figure 2 (b) shows the variation of axial displacement. Although, the axial displacement is more which is good to design for a soft actuator, but it shows negligible dependence on α i.e. one can use a smaller aspect ratio if the application requires only actuation consideration in axial direction which is generally the case. The reason for non-dependency of axial actuation is that the axial stretch is not a function of α (See, Figure 3 (b)).

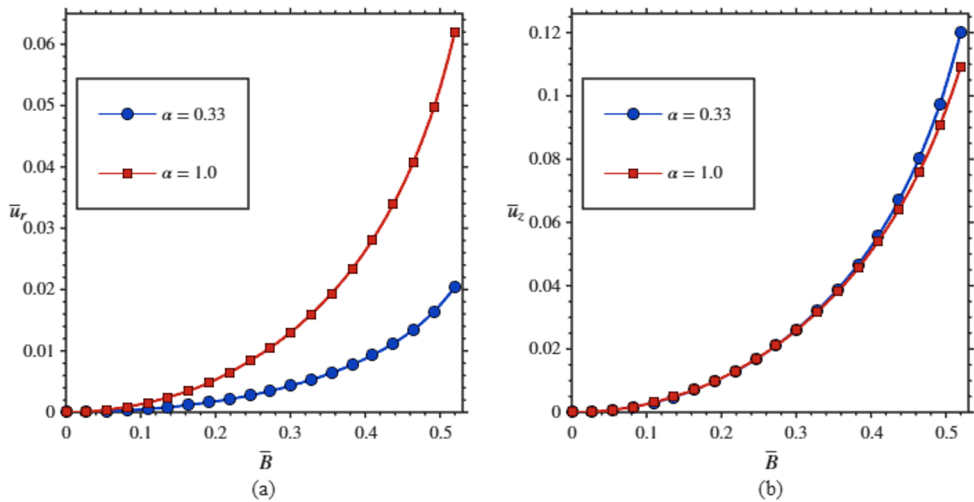


Fig. 2. Variation of the (a) normalized radial displacement \bar{u}_r and (b) normalized axial displacement \bar{u}_z as a function of the dimensionless magnetic flux density \bar{B} .

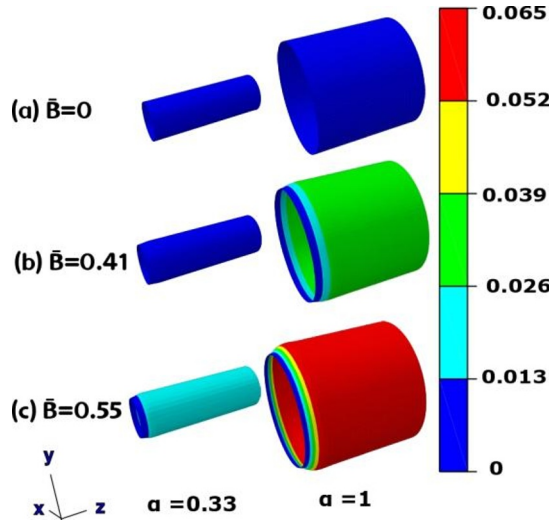


Fig. 3. Variation of the normalized radial displacement \bar{u}_r for cylindrical MRE tubes with aspect ratios $\alpha = 0.33$ and $\alpha = 1.0$, for $\bar{B} = 0, 0.41, 0.55$.

We have also plotted variation of circumferential stretch with magnetic field as can be seen in Figure 4 (a) for both cases is more than 20 % suggest very large actuation. The value of axial stretch is low in comparison to circumferential stretch.

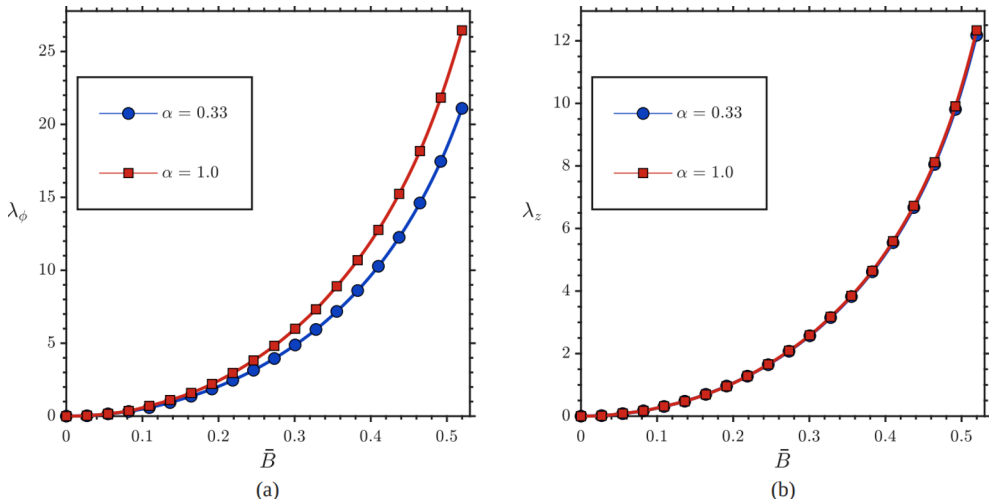


Fig. 4. Variation of the (a) circumferential λ_ϕ (%) and (b) axial λ_z (%) stretch ratios with the dimensionless magnetic flux density \bar{B} .

The visual deformation patterns corresponding to circumferential stretch are shown in Figure 5, providing a qualitative visualization of the strong circumferential expansion.

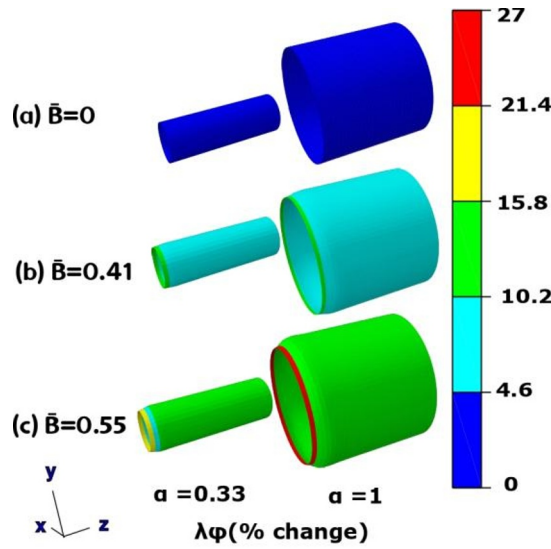


Fig. 5. Distribution of the circumferential λ_ϕ for cylindrical MRE tubes with aspect ratios $\alpha = 0.33$ and $\alpha = 1.0$, for $\bar{B} = 0, 0.41, 0.55$.

Figure 6 shows the variation of circumferential stress with increase in magnetic flux density. For higher α the $\bar{\sigma}_\phi$ is higher. The other stresses are negligible, so the results are omitted. The stresses as well as strains here show somewhat consistency with classical open tube cylindrical geometry subjected to internal pressure, i.e. circumferential strain as well as stresses are dominant though it should be verified more. The corresponding spatial stress distribution within the geometry is presented in Figure 7, showing that the maximum circumferential stress localizes near the inner perimeter for higher \bar{B} , particularly when the aspect ratio is high.

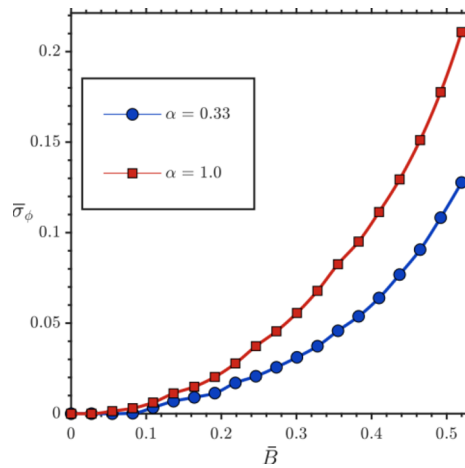


Fig. 6. Variation of the normalized circumferential stress $\bar{\sigma}_\phi$ with the dimensionless magnetic flux density \bar{B} .

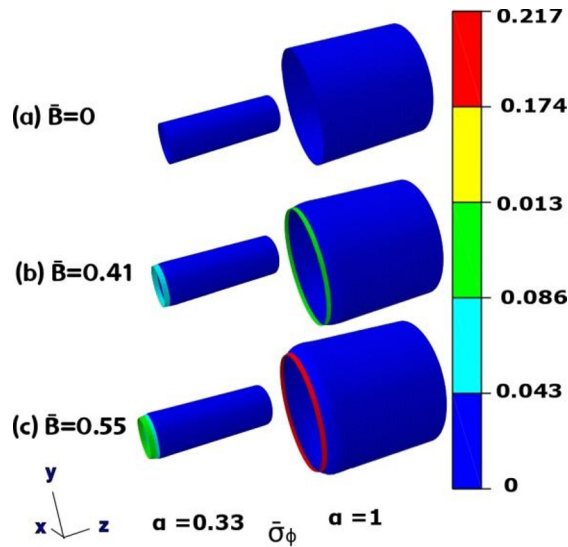


Fig. 7. Spatial distribution of normalized circumferential stress $\bar{\sigma}_\phi$ in the cylindrical tube for aspect ratios $\alpha = 0.33$ and $\alpha = 1.0$ at $\bar{B} = 0, 0.41, 0.55$.

4 Comparison with previous studies

Previous modelling efforts on magneto-elastic tubes and membranes have mostly relied on analytical or semi-analytical approaches under idealised deformation symmetries. For instance, Bustamante et al. [13] examined a thick-walled incompressible tube under magnetic and mechanical loads, obtaining numerical solutions for the finite-geometry problem, while Saxena [14] extended this configuration to capture incremental axisymmetric motions and related stability characteristics. Barreto et al. [15] further introduced analytical treatments for anisotropic thin tubes. These studies collectively provide valuable theoretical insights into magnetoelastic behaviour in cylindrical and membrane geometries, although generally in simplified loading and kinematic settings.

Numerical modelling frameworks targeting magneto-active polymers have also been explored. Haldar et al. [16] applied finite-element simulations to account for rate-dependent polymer response, while Liu et al. [17] proposed a staggered electromagnetic-mechanical numerical scheme for slender MAE structures. In Abaqus, Dohmen and Kraus [18] implemented a coupled magneto-mechanical UMAT for structured magneto-active solids. These numerical strategies are primarily aimed at fully three-dimensional formulations, typically requiring through-thickness meshing with solid elements.

The present computational approach extends this body of work by providing a thin-structure treatment of a cylindrical MAE tube, where the mechanical actuation response to a magnetic field is evaluated using shell-type elements and a magneto-elastic constitutive update. The formulation enables direct evaluation of radial expansion, circumferential and axial stretch, and stress distributions under time-dependent magnetic loading. The resulting deformation characteristics are discussed in the preceding figures and provide engineering-level interpretation of MAE tube actuation behaviour for different aspect ratios.

5 Conclusions

A numerical FE based coupled hyper-magneto-elastic method is developed for soft MREs actuators. Although, it's for Ogden material the framework is general for any other nonlinear hyper-elastic model. The cylindrical tube actuator is modeled. The study shows that to obtain actuation in axial direction one should choose a lower aspect ratio. At higher aspect ratio, circumferential stresses, strains and radial actuation is higher.

Acknowledgement: The author AS is grateful to Dr. Harpreet Singh Grewal (SNU, Dadri (India)) for using his lab facility.

References

Journal articles

1. A. K. Bastola, M. Hossain, A review on magneto-mechanical characterizations of magnetorheological elastomers. *Compos. Part B: Eng.* **200**, 108348 (2020). <https://doi.org/10.1016/j.compositesb.2020.108348>
2. S. S. Kang, K. Choi, J.-D. Nam, H. J. Choi, Magnetorheological elastomers: Fabrication, characteristics, and applications. *Mater.* **13**(20), 4597 (2020). <https://doi.org/10.3390/ma13204597>
3. A. Saber, R. Sedaghati, The modeling of magnetorheological elastomers: A state-of-the-art review. *Adv. Eng. Mater.* **25**(16), 2300182 (2023). <https://doi.org/10.1002/adem.202300182>
4. N. Bira, P. Dhagat, J. R. Davidson, A review of magnetic elastomers and their role in soft robotics. *Front. Robot. AI* **7**, 588391 (2020). <https://doi.org/10.3389/frobt.2020.588391>
5. L. Bodelot, J.-P. Voropaieff, T. Pössinger, Experimental investigation of the coupled magneto-mechanical response in magnetorheological elastomers. *Exp. Mech.* **58**(2), 207–221 (2018). <https://doi.org/10.1007/s11340-017-0334-7>
6. A. Dorfmann, R. W. Ogden, Magnetoelastic modelling of elastomers. *Eur. J. Mech. A/Solids* **22**(4), 497–507 (2003). [https://doi.org/10.1016/S0997-7538\(03\)00067-6](https://doi.org/10.1016/S0997-7538(03)00067-6)
7. J. M. Ginder, S. M. Clark, W. F. Schlotter, M. E. Nichols, Magnetostrictive phenomena in magnetorheological elastomers. *Int. J. Mod. Phys. B* **16**(17–18), 2412–2418 (2002). https://doi.org/10.1142/9789812777546_0070
8. D. Mukherjee, K. Danas, A unified dual modeling framework for soft and hard magnetorheological elastomers. *Int. J. Solids Struct.* **257**, 111513 (2022). <https://doi.org/10.1016/j.ijsolstr.2022.111513>
9. M. N. Ali, S. K. Wahi, S. Santapuri, Modeling and analysis of a magnetoelastic annular membrane placed in an azimuthal magnetic field. *Math. Mech. Solids* **26**(11), 1614–1634 (2021). <https://doi.org/10.1177/1081286521997511>
10. A. K. Srivastava, S. Basu, Exploring the performance of a dielectric elastomer generator through numerical simulations. *Sens. Actuators A: Phys.* **319**, 112401 (2021). <https://doi.org/10.1016/j.sna.2020.112401>
11. A. K. Srivastava, S. Basu, Modelling the performance of devices based on thin dielectric elastomer membranes. *Mech. Mater.* **137**, 103136 (2019). <https://doi.org/10.1016/j.mechmat.2019.103136>
12. Y. L. Raikher, O. V. Stolbov, G. V. Stepanov, Deformation of a circular ferroelastic membrane in a uniform magnetic field. *Tech. Phys.* **53**(9), 1169–1176 (2008). <https://doi.org/10.1134/S1063784208090077>

13. R. Bustamante, A. Dorfmann, R. W. Ogden, A nonlinear magnetoelastic tube under extension and inflation in an axial magnetic field: numerical solution. *J. Eng. Math.* **59**, 139–153 (2007). <https://doi.org/10.1007/s10665-006-9088-4>
14. P. Saxena, Finite deformations and incremental axisymmetric motions of a magnetoelastic tube. *Math. Mech. Solids* **23**(6), 950–983 (2018). <https://doi.org/10.1177/1081286517697502>
15. D. D. Barreto, A. Kumar, S. Santapuri, Extension–Torsion–Inflation Coupling in Compressible Magnetoelastomeric Thin Tubes with Helical Magnetic Anisotropy. *J. Elasticity* **140**, 273–302 (2020). <https://doi.org/10.1007/s10659-020-09769-6>
16. K. Haldar, B. Kiefer, A. Menzel, Finite element simulation of rate-dependent magneto-active polymer response. *Smart Mater. Struct.* **25**(10), 104003 (2016). <https://doi.org/10.1088/0964-1726/25/10/104003>
17. Y. Liu, S. Chen, X. Tan, C. Cao, A finite element framework for magneto-actuated large deformation and instability of slender magneto-active elastomers. *Int. J. Appl. Mech.* **12**(1), 2050013 (2020). <https://doi.org/10.1142/S1758825120500131>
18. E. Dohmen, B. Kraus, Coupled anisotropic magneto-mechanical material model for structured magnetoactive materials. *Polymers* **12**(11), 2710 (2020). <https://doi.org/10.3390/polym12112710>